3D modeling and measurement of HTS tape stacks in linear superconducting magnetic bearings

OPEN ACCESS
IOP Publishing
Superconductor Science and Technology
Supercond. Sci. Technol. **37** (2024) 065003 (11pp)
https://doi.org/10.1088/1361-6668/ad3c9a

3D modeling and measurement of HTS tape stacks in linear superconducting magnetic bearings

Asef Ghabeli[1,*], Günter Fuchs[2], Jens Hänisch[1], Pengbo Zhou[1,3], Oliver de Haas[2], Antonio Morandi[4] and Francesco Grilli[1]

[1] Institute for Technical Physics, Karlsruhe Institute of Technology, Karlsruhe, Germany
[2] evico GmbH, Dresden, Germany
[3] State Key Laboratory of Rail Transit Vehicle System, Southwest Jiaotong University, Chengdu, People's Republic of China
[4] University of Bologna, Bologna, Italy

E-mail: asef.ghabeli@kit.edu

Received 8 August 2023, revised 22 March 2024
Accepted for publication 9 April 2024
Published 30 April 2024

Abstract

Superconducting magnetic bearings (SMBs) are among the possible new technologies to be incorporated in maglev vehicles. Stacks of high-temperature superconductor (HTS) tapes can be used as an alternative to bulks, because stacks offer better mechanical properties, a better thermal conductivity and a simpler production process. Numerical modeling has been employed as a cost-effective, fast and reliable tool for improving the performance of SMBs. Several scenarios can be simulated with fast and relatively simple 2D models; however, in some cases using 3D models is inevitable. In this study, we use a full 3D model to solve the problem of magnetization of the tape stacks and obtaining the hysteresis force loop between a permanent magnet and the tape stacks. For this purpose, we employ an energy minimization-based method called minimum electromagnetic entropy production in 3D, combined with a homogenization technique and the $J_c(B,\theta)$ dependence of the HTS tape as input. The modeling results agree very well with the experiment both in the zero-field cooled and field-cooled conditions. The presented approach offers significant computational advantages, delivering faster and more efficient results compared to previously proposed 3D methods.

Keywords: magnetization of HTS tape stack, numerical modeling, superconducting magnetic bearing, 3D modeling

1. Introduction

Superconducting magnetic bearings (SMBs) are among the promising candidates to be employed in maglev vehicles [1]. The levitation phenomenon, which is the basic mechanism of SMB devices, is generated by the resultant repulsive force arising from the interaction between the magnetic field of a magnet guideway and the shielding current formed inside the superconducting materials. The advantage is that in field cooling condition, this force is mechanically stable without the need of any control system, unlike the repulsive force between two permanent magnets (PMs).

Bulk superconductors have been mostly employed as the passive component in SMBs [2–5]. Recently, stacks of high-temperature superconductor (HTS) tapes have been used as an

* Author to whom any correspondence should be addressed.

alternative to the bulks because they offer better mechanical properties, better thermal conductivity (thanks to the copper and silver layers in the tapes), and a rather simple production process for obtaining different shapes and sizes [6–8].

Numerical modeling can be employed as a cost-effective, fast and reliable tool to improve or optimize the performance of the SMBs. This has been the topic of several articles. For example, in [4, 9, 10] the magnet guideway was subjected to optimization or improvement while in [11, 12] the passive part of the SMB was either optimized or improved. In the optimization process, the problem should be solved in a reasonable time. This is why 2D models are more popular for these kinds of analysis [13, 14]. However, using 3D models can be inevitable under certain conditions, for example:

(i) when the depth of the problem geometry is comparable to the width and height;
(ii) when the magnet guideway or the passive component geometries are complex or without symmetries;
(iii) when certain details related to the problem depth are required.

A fast and efficient 3D model that can be solved in a reasonable time can be the solution to the above-mentioned issues. Therefore, we employ an energy minimization-based method called minimum electromagnetic entropy production method in 3D (MEMEP 3D) implemented in C++ for solving the problem of magnetization of stacks of tapes in three dimensions. This method was introduced and verified against experiments and other models by Pardo *et al* in several works [15, 16]. In [17, 18] MEMEP 3D was employed for solving the magnetization of bulks and stacks of tapes and verified against experiments, and in [19, 20] for modeling a dynamo-type flux pump in 3D with good agreement against experiments.

In this work, we developed a full 3D model based on the MEMEP 3D method using the homogenization technique and the $J_c(B,\theta)$ dependence of the HTS tape as input to calculate the levitation force between a PM and stacks of tapes in field-cooling (FC) and zero-field cooling (ZFC) cases. The significance of the presented modeling results in comparison to prior literature lies in the satisfactory calculation of levitation forces using $J_c(B,\theta)$ data obtained from independent $V-I$ characterizations and not by manually finding the best parameters of the $J_c(B,\theta)$ dependence that fit the measured maximum levitation force. With this approach, the maximum levitation forces in ZFC and FC cases show very good agreement with experiments.

2. Problem description

The passive part of the SMB is composed of two parallel stacks of SuperOx tapes, each one containing 132 tapes. In ZFC, the PM starts approaching the HTS tape stacks from a very large distance, where the PM is far enough from the tape stacks and its magnetic field is negligible, up to a minimum distance; then it goes back to its initial position in a full cycle. In FC, the PM starts its movement at a distance of 8 mm from the HTS tape stacks (where the magnetic field at tape stacks is not zero), and moves until a minimum distance; then it moves away to the distance of 50 mm, and goes back to a minimum distance in a full cycle. Figure 1 shows the schematic of the problem in the ZFC and FC cases. The parameters of the problem are tabulated in table 1. The goal of the numerical simulations is to obtain the hysteresis loop of the levitation force between the tape stacks and the PM. The force $\mathbf{F}$ is generated due to the interaction between the PM magnetic field and the screening current generated in the HTS tape stacks:

$$\mathbf{F} = \int_{\Omega} \mathbf{J} \times \mathbf{B}\, \mathrm{d}\Omega, \tag{1}$$

where Ω is the HTS domain, $\mathbf{J}$ is the screening current in the HTS tape stacks and $\mathbf{B}$ is the magnetic field of PM.

3. Calculation method

3.1. MEMEP 3D method

The MEMEP 3D method, used to model the SMB, is a variational method based on the $\mathbf{T}$-formulation, where $\mathbf{T}$ stands for effective magnetization. The effective magnetization is confined exclusively within the HTS tape stacks, resulting in a problem meshed solely inside the superconducting domains and the defined air gap between them. This feature reduces the number of degrees of freedom and hence significantly accelerates the computation [16, 17]. MEMEP solves the problem by minimizing the entropy production generated by the electromagnetic fields [16, 21]. This method is capable of modeling any combination of applied magnetic field and transport current and any $E-J$ relation. However, in the case of SMB, only the applied magnetic field caused by the PM exists, which simplifies the functional. The air gap between the two tape stacks is modeled as a conducting material with high resistivity.

MEMEP 3D solves the problem by minimizing a functional containing the variables of the problem. This functional always presents a unique minimum value, which is the only solution of the Maxwell differential equations [16]. The 3D functional is

$$L = \int_V \mathrm{d}v \left[\frac{1}{2} \frac{\Delta \mathbf{A}_J}{\Delta t} \cdot (\nabla \times \Delta \mathbf{T}) + \frac{\Delta \mathbf{A}_M}{\Delta t} \cdot (\nabla \times \Delta \mathbf{T}) + U(\nabla \times \mathbf{T}) \right], \tag{2}$$

where V is the volume of the superconducting domain, $\mathbf{T}$ is the effective magnetization, calculated as $\nabla \times \mathbf{T} = \mathbf{J}$, $\mathbf{A}_M$ and $\mathbf{A}_J$ are the vector potentials due to the applied field and due to the current density in the superconductor, respectively. $\mathbf{A}_J$ can be easily calculated with the volume integral of current density. $\mathbf{A}_M$ and $\mathbf{B}_M$ (magnetic field density of the PM) are calculated analytically at each time step and at certain points located at the center of each cell. The cylindrical PM consists of many current loops distributed uniformly along the height of the PM. $\mathbf{A}_M$ and $\mathbf{B}_M$ due to the entire PM are calculated by summing

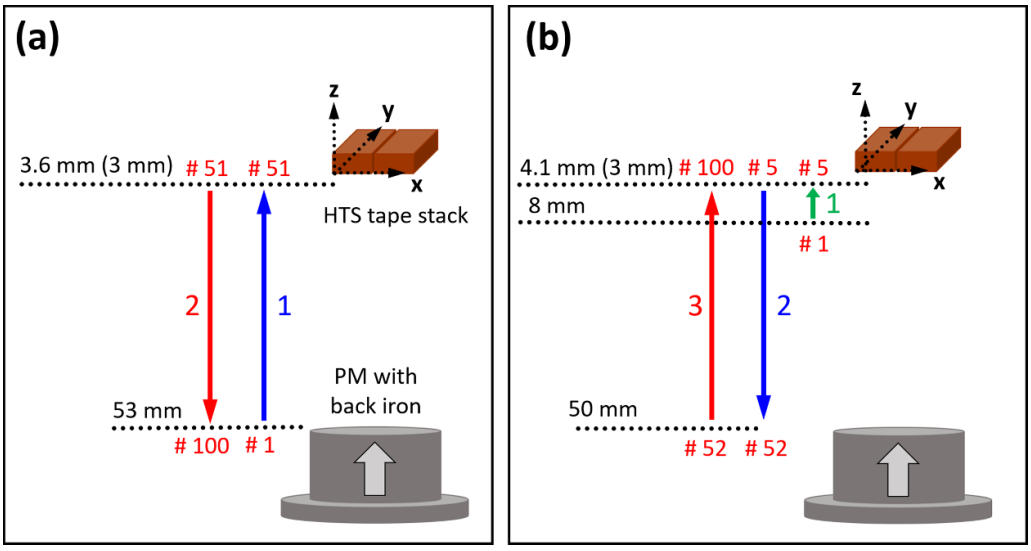

Figure 1. Schematic of the problem in (a) ZFC; (b) FC. The red numbers marked with # represent the time step number. The minimum distances in parentheses are those used in sections 5.2 and 5.3, the other ones are those used in sections 3.5 and 5.1.

Table 1. Problem parameters including PM geometry and movement and HTS tape stacks characteristics.

Permanent magnet	Diameter	35 mm
	Height	25 mm
	Remanent flux density, B_r	1.35 T
	Movement speed	10 mm s^{-1}
Magnet displacement	ZFC	3.6 mm (3 mm)[a] $< \Delta z <$ 53 mm
	FC	4.1 mm (3 mm)[a] $< \Delta z <$ 50 mm
Two stacks of tapes	Width	2 × 12 mm
	Depth	24 mm
	Height	10 mm
	air gap between stacks	≈ 1 mm
HTS tape	Width	12 mm
	Total thickness	76 μm
	Thickness of the superconducting layer	1 μm
	Self-field critical current at 77 K	399 A
	n-value	30

[a] The minimum distances in parentheses are those used in sections 5.2 and 5.3, the other ones are those used in sections 3.5 and 5.1.

up the contributions from each of these current loops [19]. U is the dissipation factor, defined as [16]

$$U(\mathbf{J}) = \int_0^{\mathbf{J}} \mathbf{E}(\mathbf{J}') \cdot \mathrm{d}\mathbf{J}'. \tag{3}$$

In our model, we used an $E-J$ power law to describe the nonlinear behavior of the HTS material as

$$\mathbf{E}(\mathbf{J}) = E_c \left(\frac{|\mathbf{J}|}{J_c(B,\theta)} \right)^n \frac{\mathbf{J}}{|\mathbf{J}|}, \tag{4}$$

where $E_c = 10^{-4}$ V m^{-1} is the critical electric field, $J_c(B,\theta)$ is the critical current density dependent on the the amplitude and direction of the magnetic field and n is the n-value of the superconducting material.

The PM had a back iron of 5 mm in height, which is not very straightforward to be implemented in the model with an analytical formula. To simplify the PM analytical model, the effect of the back iron was considered in the model by increasing the PM height by 5 mm (from 20 mm to 25 mm), without modifying the remanent magnetization of the PM. The analytical results were compared to the ones obtained by the 3D model of the PM with back iron in COMSOL Multiphysics, and there was only a 0.1% difference in the maximum magnetic field at 1 mm distance. In addition, the distribution of magnetic field agreed well with the analytical model.

3.2. Homogenization technique

We employed the homogenization technique to model the HTS tape stacks. This technique is a popular approach to model hundreds of turns in a coil or tape stack, with a high reduction of the computation time and without significant loss of

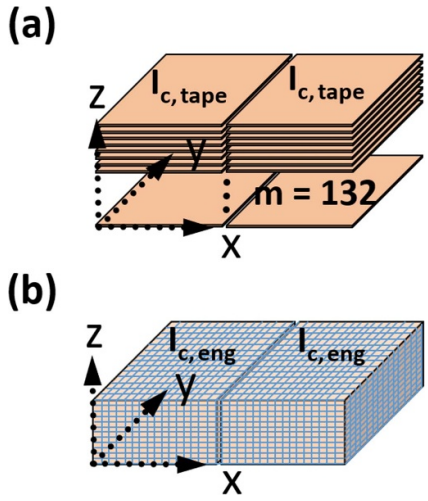

Figure 2. Homogenization of the two HTS tape stacks into two HTS bulks: (a) tape stacks; (b) homogenized meshed bulks. Mesh elements only exist inside the superconducting tape stacks and the air gap between them.

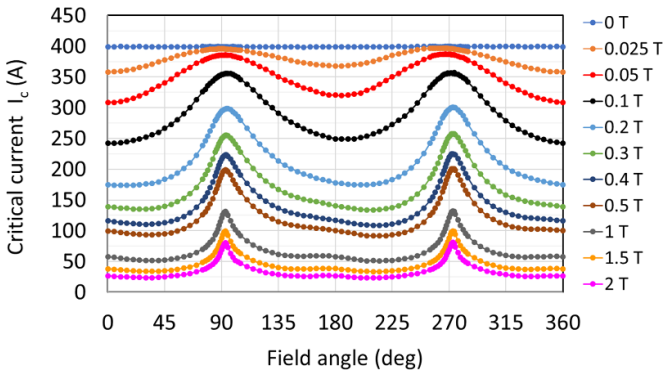

Figure 3. Measured $I_c(B,\theta)$ data of SuperOx tape at 77 K under various magnetic fields and orientations scaled to 12 mm width based on the measured I_{c0} value of 399 A on the whole 12 mm wide tape. The field angle is defined with respect to the normal vector of the tape surface. The data were provided by Robinson Research Institute in New Zealand from measurements performed at their SuperCurrent facility [27].

accuracy [22–25]. In 3D models, the homogenization technique is often inevitable, given the large number of degrees of freedom in the model [26]. In our model, we converted the two stacks of tapes, each including 132 tapes, into two homogenized bulks (see figure 2). In contrast to the bulk, in the tape stacks no current flows in the z direction (along the height of the tape stack) due to the high resistivity of the non-superconducting layers composing the tapes. In our model, we assume electrically insulated tapes, so the current density in z direction is always zero. [18]. The critical current density of the HTS tapes in the stack, $J_{c,\mathrm{tape}}$ was converted into the engineering critical current density, $J_{c,\mathrm{eng}}$, applied to the homogenized bulks as

$$J_{c,\mathrm{eng}} = m \times \frac{\delta}{\Delta_{\mathrm{bulk}}} J_{c,\mathrm{tape}} = \frac{\delta}{\Delta_{\mathrm{tape}}} J_{c,\mathrm{tape}}, \qquad (5)$$

where m is number of HTS tapes in a tape stack, δ is the thickness of the HTS layer, and Δ_{bulk} is the height of the homogenized bulks. Since m and $\Delta_{\mathrm{bulk}} = m \times \Delta_{\mathrm{tape}}$ are correlated, with changing the number of tapes in the tape stack, $J_{c,\mathrm{eng}}$ remains the same. Therefore, we can rewrite the equation based on the total thickness of just one tape, Δ_{tape}. We use this feature for investigating the impact of tape number on levitation force in section 5.3.

3.3. I_c measurement and model implementation

The coated-conductor superconducting tape used for making tape stacks is a 12 mm-wide SuperOx wire with 76 μm total thickness, consisting of 1 μm GdBCO superconducting layer, 50 μm Hastelloy 276 substrate and 1 μm of silver layer. These layers are surrounded by 10 μm copper stabilizer layer. The $I_c(B,\theta)$ characteristic of the HTS tape (see figure 3) was implemented in the model by interpolating the experimental points. The data were provided by Robinson Research Institute in New Zealand from measurements performed at their SuperCurrent facility [27].

The I_c data were measured on a sample with dimensions of 0.5 mm × 5 mm (width × length) cut from the central part of the tape in order to easily measure the high value of critical current in the tape. The measured critical current of the 0.5 mm wide sample at self-field was 19.29 A, which would correspond to an I_{c0} of 463 A for the 12 mm wide tape. However, this simple scaling is often inaccurate, due to the fact that the critical current is not homogeneous across the width of the tape. The lateral inhomogeneity of the critical current across the tape width in coated-conductors has been reported and investigated in several articles [28–33]. Those studies showed that the central part of the tape has usually higher critical current than the lateral parts. That is why measuring I_c on a 0.5 mm wide sample cut from the central part of the tape and scaling it to 12 mm width can not provide an accurate representation of I_c on the 12 mm wide tape. For this reason, we also measured I_{c0} on the 12 mm wide tape at self-field and obtained the value of 399 A at 77 K, which is around 14% lower than the scaled I_c. Afterwards, we scaled the set of $I_c(B,\theta)$ data for 0.5 mm wide tape under various magnetic fields and orientations according to the measured I_{c0} of 399 A, i.e. by a factor (12 mm/0.5 mm)/(463 A/399 A) = 20.69 (see figure 3). This means that for example, according to equation (5) and the values presented in table 1, the self-field engineering critical current density of the homogenized bulk, $J_{c0,\mathrm{eng}}$, is 4.375×10^8 A m^{-2}.

3.4. Meshing and calculation time

As mentioned before, meshing is only necessary inside the sample (see figure 2(b)). For the two HTS tape stacks with the dimensions of 24 × 24 × 10 mm in x, y and z directions, we used 31 × 31 × 13 elements, respectively. One of the 31 mesh

elements in x is assigned to the air gap between the two tape stacks. Each millimeter of PM movement was considered as one time step. We found that increasing the number of mesh elements and time steps changes the output result only negligibly. With a total number of 12 493 mesh elements, using 100 time steps, and on a computer with the specification of AMD Ryzen threadripper 3970x 32-core processor, 128 GB RAM, and Ubuntu 20.04.4 LTS operating system, the calculation times for one full cycle of the ZFC and FC cases were 4 h and 4 h and 31 min, respectively.

3.5. Model validation

Before comparing our model with experiments, we validated it against the 3D segregated $\boldsymbol{H}$-formulation method implemented in COMSOL Multiphysics. The segregated $\boldsymbol{H}$-formulation method was firstly developed and used by Quéval *et al* to model the ZFC and FC cases of a SMB in 2D and 3D [4, 26]. In short, the model is composed of two separate parts, namely a magnetostatic model to solve the magnetic field of the PM and a time-dependent $\boldsymbol{H}$-formulation for the HTS tape stacks. The latter uses the magnetic field calculated by the former as input. This approach eliminates the need of a moving mesh and reduces the number of degrees of freedom in the time-dependent model [34–36].

The problem configuration used for the comparison is similar to the one presented in section 2, with the difference that, for simplicity, the air gap between the two bulks is disregarded, and the two bulks and the air gap between them is modeled as one simple bulk with dimensions of 24 $\times$ 24 $\times$ 10 mm. For the bulk in x, y and z directions, we used 30 $\times$ 30 $\times$ 13 elements. In addition, a constant J_c was used in the model.

Figure 4 shows that there is a very good agreement between the calculated levitation forces of the 3D Segregated $\boldsymbol{H}$-formulation method and MEMEP 3D in ZFC mode, with only 1.5% difference in the calculated maximum levitation forces. The calculation times for 3D MEMEP method and 3D segregated $\boldsymbol{H}$-formulation, using the same computer mentioned in section 3.4 were 1 h and 10 min, and 15 h and 44 min, respectively. Although the calculation time with a mesh of 17 $\times$ 17 $\times$ 5 elements was very short (around 3 min) for both methods, with a higher numbers of elements MEMEP 3D showed a clear computational advantage.

4. Force measurements

Two HTS tape stacks were prepared from 24 mm long pieces of the GdBCO coated-conductor tape by stacking 2 $\times$ 132 HTS tape pieces. The two stacks, around 10 mm in height, were assembled in a box prepared from glass fiber reinforced plastic (GRP) as shown in figure 5(a). A GRP top was fixed to the box by screws. The stacks were carefully compressed at room temperature using screws. This compression remains almost unchanged during cooling from room temperature to 77 K, because of the similar thermal contraction $\Delta L/L \approx 0.2\,\%$ for GRP and the Hastelloy 276 substrate of the HTS tapes.

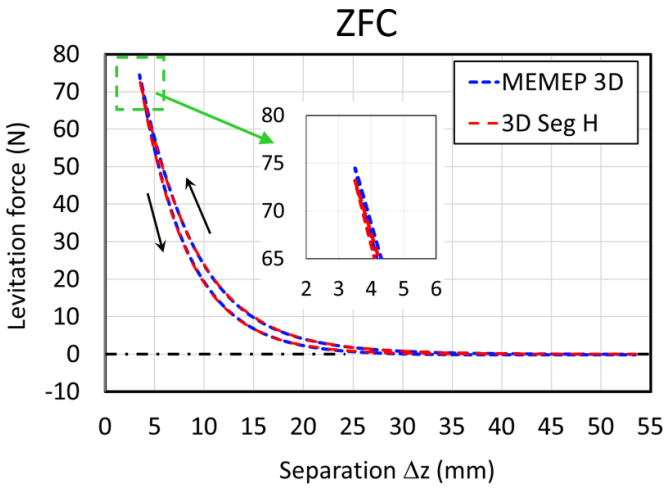

Figure 4. Comparison between the calculated levitation forces as a function of separation between the PM and HTS tape stacks of 3D Segregated $\boldsymbol{H}$-formulation method and MEMEP 3D during the first cycle in ZFC mode.

The GRP box with the stacks was fixed to the frame of the setup for the force measurement and cooled by liquid nitrogen. The NdFeB PM with back iron was vertically moved above the stacks along the axis of the stacks. The force between the PM and the stacks was measured by a force sensor (AEP transducer, type TCA, maximum force 100 N). The position of the PM was measured by a resistive displacement sensor (Type FWA100T), which is designed for a maximal vertical displacement of 100 mm. Such a sensor has a small error of $\Delta z = \pm$ 0.085 mm, even for small values of z. Force and displacement data were synchronized by an ALMEMO data logger in order to measure the levitation force of the HTS tape stack based on the distance between the magnet and the superconductor.

Before starting the force measurement, the HTS tape stacks were cooled to 77 K, at a large distance of 53 mm from the PM (ZFC), or in the presence of an applied field at the cooling distance of 8 mm between the superconductor and the PM (FC). After ZFC, the distance Δz between the PM and superconductor was reduced stepwise starting from 53 mm.

5. Modeling results

5.1. Hysteresis loop of levitation force

As clearly seen in figures 6(a) and (b), there is a very good agreement not only in the maximum amount of levitation forces, but also in hysteresis loops between the calculated and measured levitation forces during the first cycle in ZFC and FC. The maximum levitation forces in ZFC and FC have a relative error of about 5% in comparison to experiments. The strong hysteretic behaviour of the first cycle in ZFC and even more in FC is due to magnetic flux penetrating the superconductor at a small distance between the superconductor and PM. This pinned magnetic flux within the superconductor is responsible for an attractive force (negative force values). The calculated maximum attractive force is -1.35 N for the ZFC case (against -2.6 N obtained by measurement), and -7.3 N

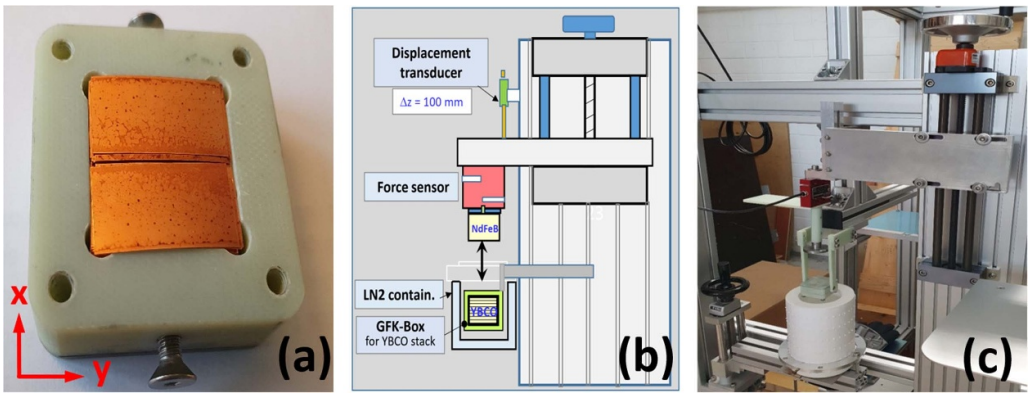

Figure 5. (a) The open GRP box with two HTS tape stacks used for the levitation force measurements; (b) schematic of the levitation force measurement setup; (c) levitation force measurement setup of the SMB.

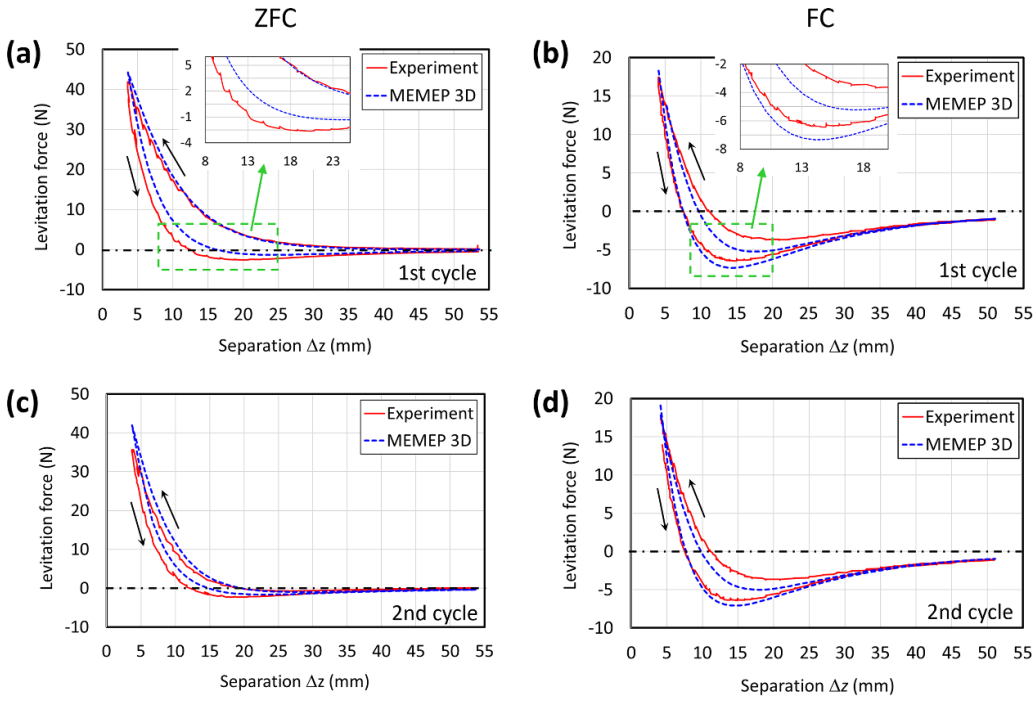

Figure 6. Comparison between the calculated and measured levitation force as a function of separation between the PM and HTS tape stacks (a) during the first cycle in ZFC mode; (b) during the first cycle in FC mode; (c) during the second cycle in ZFC mode; (d) during the second cycle in FC mode. In FC mode, the first section of displacement (between 8 mm and 4.1 mm) is not shown.

for the FC case (against −6.5 N obtained by measurement). This attractive force reduces the repulsive force in the next cycle. In FC, a large part of the hysteresis loop is dominated by the attractive force, which remains in the superconductor after the field cooling process. In ZFC, the share of the attractive force to the repulsive force in the hysteresis loop is much smaller.

Figures 6(c) and (d) show the comparison between the calculated and measured levitation forces during the second cycle in ZFC and FC, respectively. In FC, the model agrees well with the experiment, confirming that the maximum levitation force during the second cycle stays almost the same as in the first cycle. In contrast to FC, in ZFC we observe a reduction of the maximum levitation force both in the simulation and in the experiment. This reduction is higher in the experiment. The first reason lies in the difference between the maximum repulsive force of the experiment and the simulation in the first cycle, which is accumulated in the second cycle. The second and the more important reason can be attributed to the difference in the attractive forces (negative force values) in the first cycle between the simulation and experiment. The higher attractive force in the first cycle leads to a stronger reduction of the maximum repulsive force in the second cycle.

5.2. *Screening current distribution*

For a fair comparison of screening current distribution between the ZFC and FC modes, unlike the previously presented results, we considered the minimum distance of 3 mm for

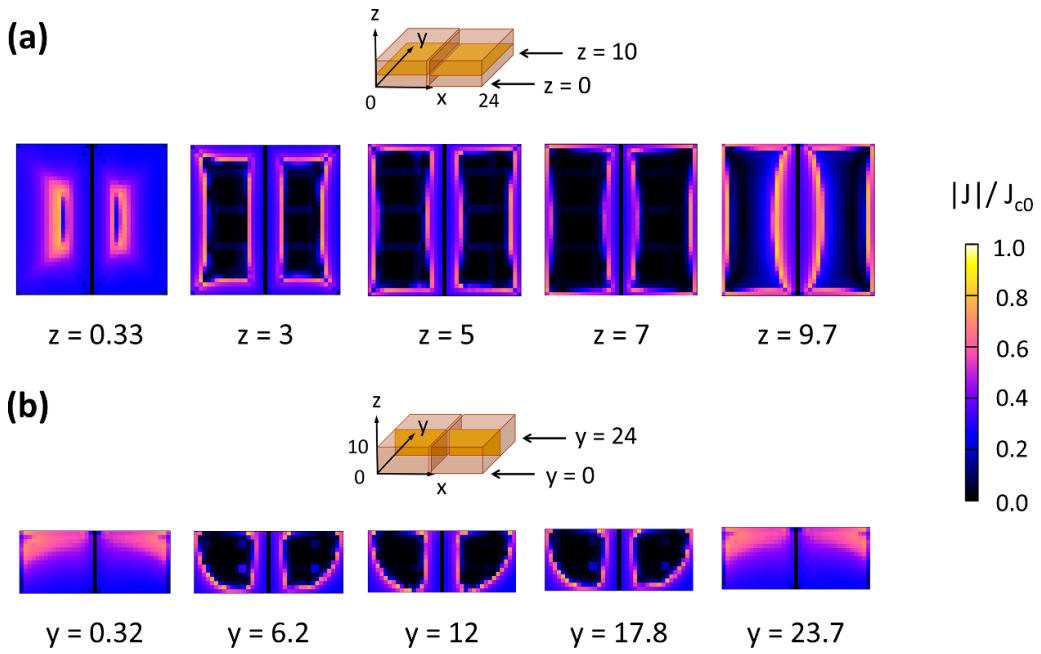

Figure 7. Screening current distribution normalized by J_{c0} in ZFC mode when the PM is in the closest distance to tape stacks (3 mm) (a) in various z-planes; (b) in various y-planes. All numbers represent positions in mm.

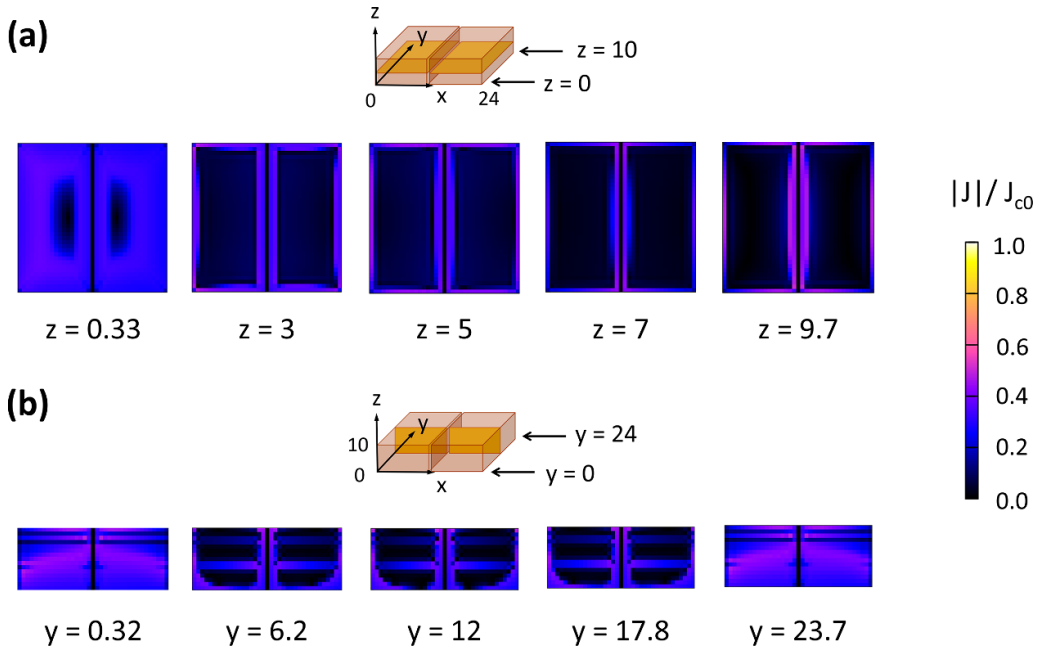

Figure 8. Screening current distribution normalized by J_{c0} in FC mode when the PM is in the closest distance to tape stacks (3 mm) (a) in various z-planes; (b) in various y-planes. All numbers represent positions in mm.

both cases. Figures 7 and 8 show the screening current distribution in ZFC and FC mode, respectively, normalized by the self-field critical current density in various z-planes and y-planes in the HTS tape stacks at the moment when the PM is at the closest distance from the tape stacks for the first time. In order to have a higher resolution for these figures, we used $37\times37\times15$ elements. In figure 7 and at this time step, the highest amount of screening current and hence shielding effect in ZFC can be seen. This causes only a small amount of PM flux to enter the superconductor, so the trapped field is very low. Farther from the PM and at higher z-plane values, the screening current flows at the edges, while as we approach the lower values of z-plane, the screening current tends to flow in the central regions. This is in agreement with the Bean model approximation for bulk superconductors [37]. In figure 8 for FC, the amount of screening current and thence the levitation force magnitude are lower than for ZFC. This is because in FC a higher amount of PM flux penetrates the superconductor, so the screening current is smaller and hence the trapped field is larger [38].

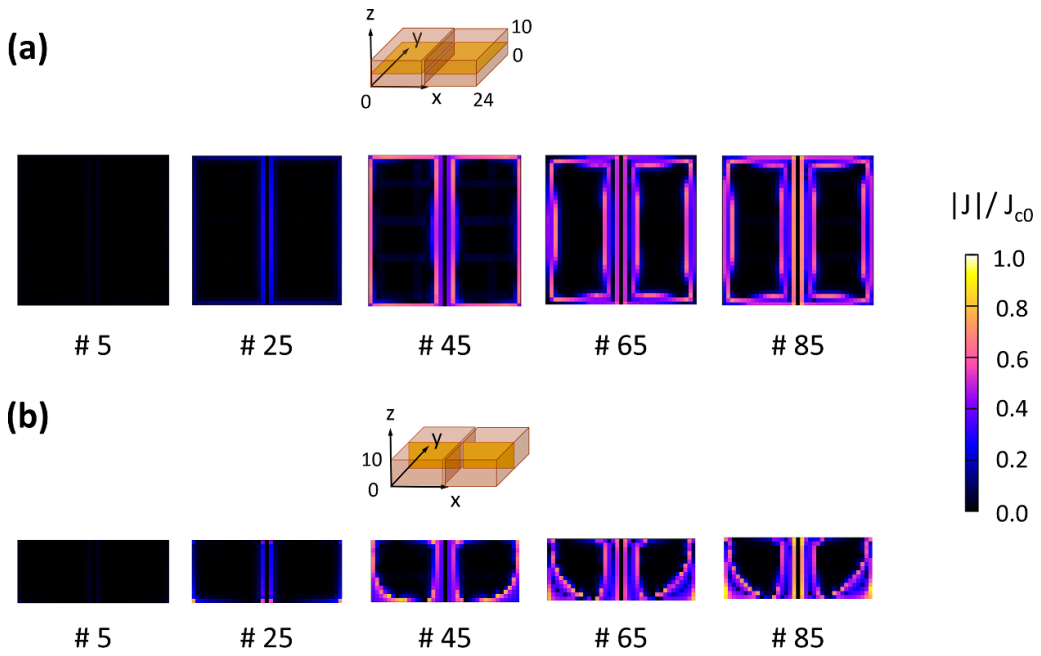

Figure 9. Screening current distribution normalized by J_{c0} in ZFC mode for various time steps during the first cycle (a) in z-plane = 5 mm, (b) in y-plane = 12 mm. # represents the time step number (see figure 1(a)).

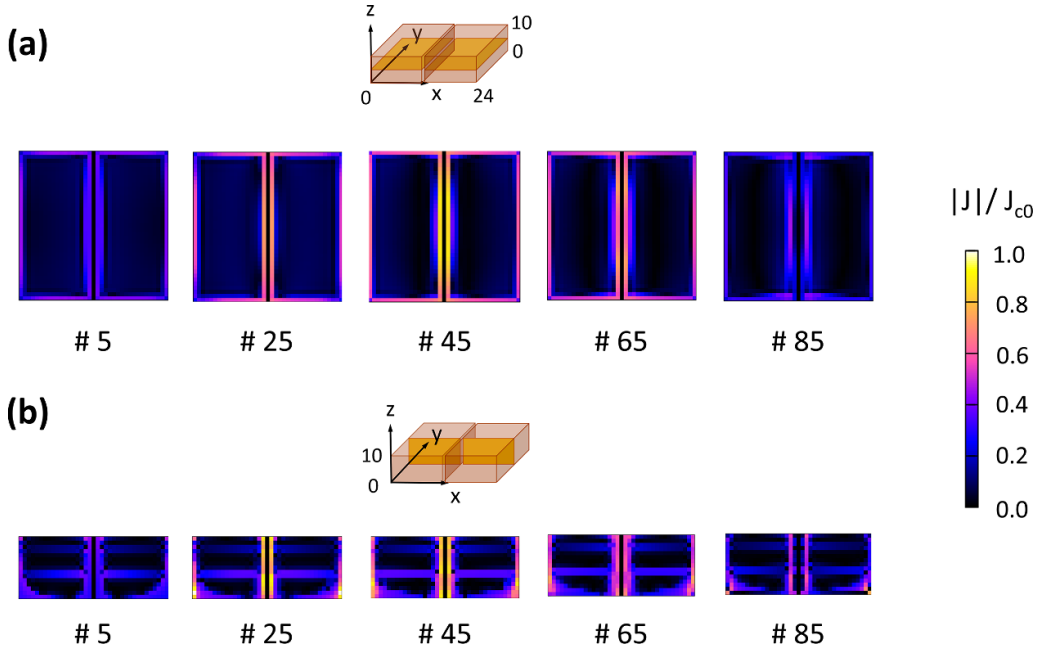

Figure 10. Screening current distribution normalized by J_{c0} in FC mode for various time steps during the first cycle (a) in z-plane = 5 mm, (b) in y-plane = 12 mm. # represents the time step number (see figure 1(b)).

Figures 9 and 10 show the screening current distribution normalized by the self-field critical current density for various time steps during the first cycle of PM excursion in ZFC and FC, respectively. In ZFC mode, as the PM approaches the tape stacks, the field becomes stronger to penetrate the stacks more deeply. In FC mode, the field has already penetrated the tape stacks in the center at time step No. 5, because the PM was already at the closest distance from the tape stacks at time step No. 4.

5.3. Impact of number of tapes on levitation force

For possible further improvement, we numerically investigated the impact of the number of tapes in the stacks on the maximum levitation force. While we kept the tape thickness constant, we changed the height of the stacks by only changing the number of tapes in them. As a result, the engineering current density is kept the same (see equation (5)). In addition, we used the same modeling technique and parameters

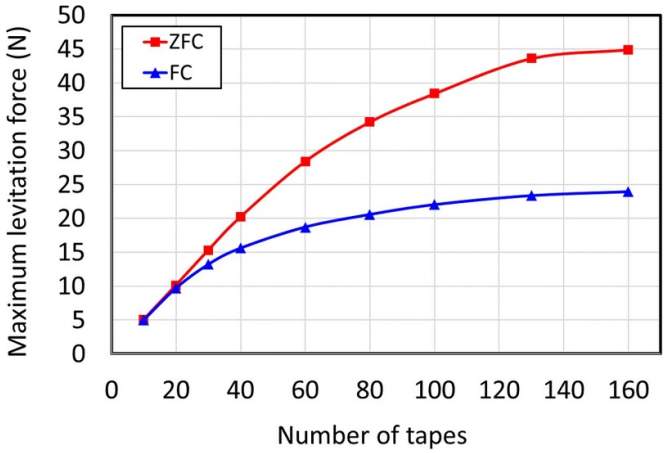

Figure 11. Maximum levitation force with respect to number of tapes in each HTS tape stack for ZFC and FC modes.

discussed above. For a fair comparison between the forces in the FC and ZFC modes, we selected a minimum distance of 3 mm for both cases. Figure 11 shows the obtained results for ZFC and FC from 10 tapes to 160 tapes in a stack (i.e. a total of 20 to 320 tapes). After around 130 tapes in a stack, the maximum levitation force saturates. This indicates that the magnetic field of the PM at 3 mm cannot penetrate the tapes any deeper. The obtained trend is in agreement with measurements performed in [7]. The screening current is formed only inside the 130 tapes that are closer to the PM and the generated screening current in the remaining tapes is negligible. In order to have a stronger levitation force with the same HTS tapes, either the magnetic field density of PM should be increased or the minimum gap between the tape stacks and the PM should be decreased. Another practical way is to use tapes with less total thickness in a stack (i.e. with thinner substrate and higher engineering current density), so that more tapes can be placed in the region where the field of the PM is strong enough to penetrate the tapes.

6. Conclusion

In this work, we developed an energy-minimization-based model called MEMEP 3D implemented in C++ to calculate the levitation force between a PM and stacks of tapes in FC and ZFC cases using the homogenization technique and the actual $J_c(B,\theta)$ dependence of the HTS tapes as input. This represents the first full 3D model to address such a problem. The hysteresis graph in both ZFC and FC shows very good agreement with experiments. This is possible by considering and implementing the appropriately scaled actual $J_c(B,\theta)$ data into the 3D model. We showed and discussed the screening current distribution in various planes of the stacks and at various time steps. This analysis gave insight into how the screening current is generated inside the stacks at different moments during the magnetization process. Moreover, we calculated the impact of the number of tapes in a stack on the obtained levitation force. The results showed that after a particular number of tapes in the stacks (in our case, 130), the magnetic field of the PM is not strong enough to fully penetrate the tapes. This causes the maximum levitation force to saturate after a certain number of tapes. In summary, the presented 3D model, taking advantage of its fast computational speed and versatility, is a promising approach to perform further investigation and improvement in the performance of SMBs.

Data availability statement

All data that support the findings of this study are included within the article (and any supplementary files).

Acknowledgment

The authors would like to acknowledge the financial support of the German Federal Ministry for Economic Affairs and Energy Under BMWi Contract No. ZIM KK5082301SH0. Additionally, the authors extend their gratitude to Wenjiao Yang from Guangdong Ocean University for the assistance with the 3D segregated $\boldsymbol{H}$-formulation model. They also express appreciation to Andres E Pantoja (Robinson Research Institute, Victoria University of Wellington) for the $I_c(B,\theta)$ measurements of the HTS tape. Last but not least, the authors are grateful to Milan Kapolka for his assistance and support for the 3D MEMEP method.

ORCID iDs

Asef Ghabeli https://orcid.org/0000-0001-9907-4509
Jens Hänisch https://orcid.org/0000-0003-2757-236X
Pengbo Zhou https://orcid.org/0000-0002-4051-1898
Antonio Morandi https://orcid.org/0000-0002-1845-4006
Francesco Grilli https://orcid.org/0000-0003-0108-7235

References

[1] Bernstein P and Noudem J 2020 Superconducting magnetic levitation: principle, materials, physics and models *Supercond. Sci. Technol.* **33** 033001
[2] Dias D H N, Motta E S, Sotelo G G, de Andrade R, Stephan R M, Kuehn L, de Haas O and Schultz L 2009

Simulations and tests of superconducting linear bearings for a MAGLEV prototype *IEEE Trans. Appl. Supercond.* **19** 2120–3
[3] Werfel F N, Floegel-Delor U, Rothfeld R, Riedel T, Wippich D, Goebel B and Schirrmeister P 2012 Bulk superconductors in mobile application *Phys. Proc.* **36** 948–52
[4] Quéval L, Sotelo G G, Kharmiz Y, Dias D H N, Sass F, Zermeño V M R and Gottkehaskamp R 2016 Optimization of the superconducting linear magnetic bearing of a maglev vehicle *IEEE Trans. Appl. Supercond.* **26** 1–5
[5] Werfel F N, Floegel-Delor U, Rothfeld R, Riedel T, Goebel B, Wippich D and Schirrmeister P 2011 Superconductor bearings, flywheels and transportation *Supercond. Sci. Technol.* **25** 014007
[6] Patel A, Hahn S, Voccio J, Baskys A, Hopkins S C and Glowacki B A 2016 Magnetic levitation using a stack of high temperature superconducting tape annuli *Supercond. Sci. Technol.* **30** 024007
[7] Osipov M, Starikovskii A, Abin D and Rudnev I 2019 Influence of the critical current on the levitation force of stacks of coated conductor superconducting tapes *Supercond. Sci. Technol.* **32** 054003
[8] Liu Z, Yang W, Yu L, Ji Y, Bai M, Li X and *et al* 2020 Testing and comparison of levitation forces and rotational friction in different superconducting tape stacks *J. Supercond. Nov. Magn.* **33** 3035–41
[9] Yang W, Quéval L, Li G, Yao C and Ma G 2020 Comparison of linear superconducting magnetic bearings using isotropic and anisotropic materials *IEEE Trans. Appl. Supercond.* **30** 1–5
[10] Zhang J, Zeng Y, Cheng J and Tang X 2008 Optimization of permanent magnet guideway for HTS maglev vehicle with numerical methods *IEEE Trans. Appl. Supercond.* **18** 1681–6
[11] Sass F, Dias D H N, Sotelo G G and de Andrade R 2012 Superconducting levitation using coated conductors *IEEE Trans. Appl. Supercond.* **23** 3600905
[12] Del-Valle N, Sanchez A, Navau C and Chen D 2010 Towards an optimized magnet-superconductor configuration in actual maglev devices *IEEE Trans. Appl. Supercond.* **21** 1469–72
[13] Ainslie M D and Fujishiro H 2015 Modelling of bulk superconductor magnetization *Supercond. Sci. Technol.* **28** 053002
[14] Grilli F, Morandi A, De Silvestri F and Brambilla R 2018 Dynamic modeling of levitation of a superconducting bulk by coupled H-magnetic field and arbitrary lagrangian-eulerian formulations *Supercond. Sci. Technol.* **31** 125003
[15] Pardo E, Kapolka M, Kováč J, Šouc J, Grilli F and Piqué A 2016 Three-dimensional modeling and measurement of coupling AC loss in soldered tapes and striated coated conductors *IEEE Trans. Appl. Supercond.* **26** 1–7
[16] Pardo E and Kapolka M 2017 3D computation of non-linear eddy currents: variational method and superconducting cubic bulk *J. Comput. Phys.* **344** 339–63
[17] Kapolka M, Pardo E, Grilli F, Baskys A, Climente-Alarcon V, Dadhich A and Glowacki B A 2020 Cross-field demagnetization of stacks of tapes: 3D modelling and measurements *Supercond. Sci. Technol.* **33** 044019
[18] Kapolka M, Zermeño V M R, Zou S, Morandi A, Ribani P L, Pardo E and Grilli F 2018 Three-dimensional modeling of the magnetization of superconducting rectangular-based bulks and tape stacks *IEEE Trans. Appl. Supercond.* **28** 8201206
[19] Ghabeli A, Pardo E and Kapolka M 2021 3D modeling of a superconducting dynamo-type flux pump *Sci. Rep.* **11** 1–12
[20] Zhou P, Ghabeli A, Ainslie M D and Grilli F 2023 Characterization of flux pump-charging of high-temperature superconducting coils using coupled numerical models *Supercond. Sci. Technol.* **36** 115002
[21] Pardo E, Šouc J and Frolek L 2015 Electromagnetic modelling of superconductors with a smooth current–voltage relation: variational principle and coils from a few turns to large magnets *Supercond. Sci. Technol.* **28** 044003
[22] Berrospe J E, Zermeño V M R, Trillaud F and Grilli F 2019 Real-time simulation of large-scale hts systems: multi-scale and homogeneous models using the T-A formulation *Supercond. Sci. Technol.* **32** 065003
[23] Berrospe J E, Trillaud F, Zermeño V M R and Grilli F 2021 Advanced electromagnetic modeling of large-scale high-temperature superconductor systems based on H and T-A formulations *Supercond. Sci. Technol.* **34** 044002
[24] Zhou P, Dos Santos G, Ghabeli A, Grilli F and Ma G 2022 Coupling electromagnetic numerical models of HTS coils to electrical circuits: multi-scale and homogeneous methodologies using the T-A formulation *Supercond. Sci. Technol.* **35** 115005
[25] Santos B M O, Dias F J M, Sass F, Sotelo G G, Polasek A and de Andrade R 2020 Simulation of superconducting machine with stacks of coated conductors using hybrid A-H formulation *IEEE Trans. Appl. Supercond.* **30** 1–9
[26] Quéval L, Liu K, Yang W, Zermeño V M R and Ma G 2018 Superconducting magnetic bearings simulation using an H-formulation finite element model *Supercond. Sci. Technol.* **31** 084001
[27] Strickland N M, Hoffmann C and Wimbush S C 2014 A 1 kA-class cryogen-free critical current characterization system for superconducting coated conductors *Rev. Sci. Instrum.* **85** 113907
[28] Solovyov M, Pardo E, Šouc J, Gömöry F, Skarba M, Konopka P, Pekarčíková M and Janovec J 2013 Non-uniformity of coated conductor tapes *Supercond. Sci. Technol.* **26** 115013
[29] Gömöry F, Šouc J, Pardo E, Seiler E, Soloviov M, Frolek L, Skarba M, Konopka P, Pekarčíková M and Janovec J 2013 AC loss in pancake coil made from 12 mm wide REBCO tape *IEEE Trans. Appl. Supercond.* **23** 5900406
[30] Amemiya N, Maruyama O, Mori M, Kashima N, Watanabe T, Nagaya S and Shiohara Y 2006 Lateral J_c distribution of YBCO coated conductors fabricated by IBAD/MOCVD process *Physica* C **445–448** 712–716
[31] Tsukamoto O 2005 AC losses in a type II superconductor strip with inhomogeneous critical current distribution *Supercond. Sci. Technol.* **18** 596
[32] Polak M, Pardo E, Mozola P and Šouc J 2012 Magnetic field in the winding of an YBCO pancake coil: experiments and calculations *IEEE Trans. Appl. Supercond.* **22** 6600204
[33] Hänisch J, Mueller F M, Ashworth S, Coulter J Y and Matias V 2008 Measurement of the transverse J_c profiles of coated conductors using a magnetic knife of permanent magnets *Supercond. Sci. Technol.* **21** 115021
[34] Yang W, Quéval L, Ma G, Ye C, Li G and Gong T 2020 A 3-D strong-coupled electromagnetic-thermal model for HTS bulk and its uses to study the dynamic characteristics of a linear HTS maglev bearing *IEEE Trans. Appl. Supercond.* **30** 1–14
[35] Yang W, Quéval L and Ma G 2022 Numerical studies of dynamic characteristics of a stack-type HTS maglev system

based on H-formulation *IEEE Trans. Appl. Supercond.* **32** 1–4
[36] Yang W, Ma G, Wang M, Zhao Z, Jia B and Xu Y 2024 Studies of the effect of copper layer on dynamic characteristics of a stack-type HTS maglev system based on H-formulation *IEEE Trans. Appl. Supercond.* **34** 1–5
[37] Ainslie M and Fujishiro H 2019 *Numerical modelling of bulk superconductor magnetisation* (IOP Publishing) pp 2053–563
[38] Costa Branco P J and Dente J A 2012 Design and experiment of a new maglev design using zero-field-cooled YBCO superconductors *IEEE Trans. Ind. Electron.* **59** 4120–7